LETTER OPEN

Check for updates

Evolution of T-cell fitness through AML progression: enhanced bispecific T-cell engager-mediated function of bone marrow T cells at remission compared to initial diagnosis and relapse

Maryam Kazerani[1,2], Anetta Marcinek[1,2], Nora Philipp[1,2], Bettina Brauchle[1,2], Jonathan Jonas Taylor[1,2], Helena Domínguez Moreno[3], Andrea Terrasi[3], Benjamin Tast[1,2], Lisa Rohrbacher[1,2], Yingshuai Wang[1,2], Maximilian Warm[2], Alica-Joana Emhardt[2], Giulia Magno[2], Karsten Spiekermann[2,4,5], Tobias Herold[2], Tobias Straub[6], Sebastian Theurich[1,2], Gunnar Schotta[3], Roman Kischel[7,8], Veit L. Bücklein[1,2] and Marion Subklewe[1,2,5]✉

Leukemia (2024) 38:2270–2275; https://doi.org/10.1038/s41375-024-02387-4

TO THE EDITOR:

In acute myeloid leukemia (AML), the anti-leukemic potential of allogeneic hematopoietic stem cell transplantation (allo-HSCT) and post-transplant donor lymphocyte infusion (DLI) hinges on the activity of T cells [1]. Bispecific antibodies, including bispecific T-cell-engager (BiTE®) molecules, redirect endogenous T cells against neoplastic cells for eradication by CD3-dependent T-cell activation. In B-lymphoid malignancies, high clinical efficacy has led to the approval of several T-cell-recruiting constructs [2, 3]. In AML, several bispecific antibodies have been developed and have shown strong preclinical efficacy [4, 5]. However, albeit early-phase I/II clinical trials in heavily pre-treated patients with R/R AML have yielded promising, dose-dependent results, sustained responses were not observed [6–8].

We hypothesize that T-cell dysfunction contributes to BiTE resistance and a lack of long-term responses in AML. Evidence for the relevance of T-cell fitness to BiTE-mediated activity is derived from patients with B-cell precursor acute lymphoblastic leukemia in whom a predominance of T cells with an exhausted phenotype was associated with failure of blinatumomab treatment [9]. Additionally, transcriptional profiles associated with T-cell dysfunction were found in nonresponding patients [10]. Further evidence of an association between T-cell fitness and BiTE activity was found in a preclinical model of T-cell exhaustion after continuous BiTE exposure [11].

So far, attempts to characterize T-cell phenotype and function in AML patients have yielded variable and sometimes contradictory results. Studies suggest that BM T cells in contrast to peripheral blood T cells better reflect the immune state and are the main mediators of BiTE-mediated cytotoxicity [12, 13]. Hence, characterizing BM T cells at different time points during the course of the disease might help to guide the optimal clinical application of T-cell-based immunotherapies in AML.

We assessed BM T cells of AML patients at initial diagnosis (ID), complete remission (CR), and first relapse (RL). All AML samples were allo-HSCT naive, and age-matched HD samples served as a control cohort (Supplementary Table 1). The percentage of BM $CD3^+$ T cells was lower at ID and RL compared to time of CR and in HD samples (Supplementary Fig. S1A–C). Of the $CD3^+$ T-cell subpopulations, the most significant changes in the T-cell differentiation states were observed in $CD8^+$ T cells (Fig. 1A, Supplementary Fig. S1D, E). Terminally differentiated effector cells (T_{EMRA}) were the most abundant population at ID compared to other time points. A higher proportion of central memory (T_{CM}) cells was apparent at RL compared to ID and CR. By contrast, a higher percentage of naive T cells (T_{Naive}) was found at CR than at ID and RL (Fig. 1A).

We next measured the expression of inhibitory receptors within the $CD4^+$ and $CD8^+$ T cell compartments during AML progression and compared them to HD T cells. A significantly higher proportion of CD244 and TIM-3 expressing cells were detected for both $CD4^+$ and $CD8^+$ patient T cells. Next, we observed a higher percentage of PD-1^+ and LAG-3^+ cells on $CD8^+$ patient T cells relative to HDs. In addition, $CD8^+$ T cells at ID showed a higher frequency of $CD160^+$ cells compared to cells from HDs. Within the $CD4^+$ T-cell compartment, we observed a lower proportion of LAG-3^+ cells at ID compared to RL. In summary, AML patients showed significantly higher expression of exhaustion-associated inhibitory receptors compared to HDs (Fig. 1B, Supplementary Fig. S1F).

To characterize the transcriptional program of AML T cells, we performed longitudinal RNA-seq analysis of sorted BM $CD3^+$ T cells from paired ID–RL samples ($n = 7$) and HDs ($n = 2$). We first compared the transcriptional profiles of T cells at both ID and RL to those of HDs and identified 1482 and 1029 differentially expressed genes (DEGs; $\log_2FC > 1$ or < -1,

[1]Laboratory for Translational Cancer Immunology, LMU Gene Center, Munich, Germany. [2]Department of Medicine III, University Hospital, LMU Munich, Munich, Germany. [3]Division of Molecular Biology, Biomedical Center, Faculty of Medicine, LMU Munich, Martinsried, Germany. [4]Experimental Leukemia and Lymphoma Research (ELLF), Department of Internal Medicine III, University Hospital, LMU Munich, Munich, Germany. [5]German Cancer Consortium (DKTK) and German Cancer Research Center (DKFZ), Heidelberg, Germany. [6]Bioinformatics Unit, Biomedical Center, LMU Munich, Martinsried, Germany. [7]Amgen Research (Munich) GmbH, Munich, Germany. [8]AMGEN Inc., Thousand Oaks, CA, USA. ✉email: Marion.Subklewe@med.uni-muenchen.de

Received: 13 March 2024 Revised: 5 August 2024 Accepted: 14 August 2024
Published online: 22 August 2024

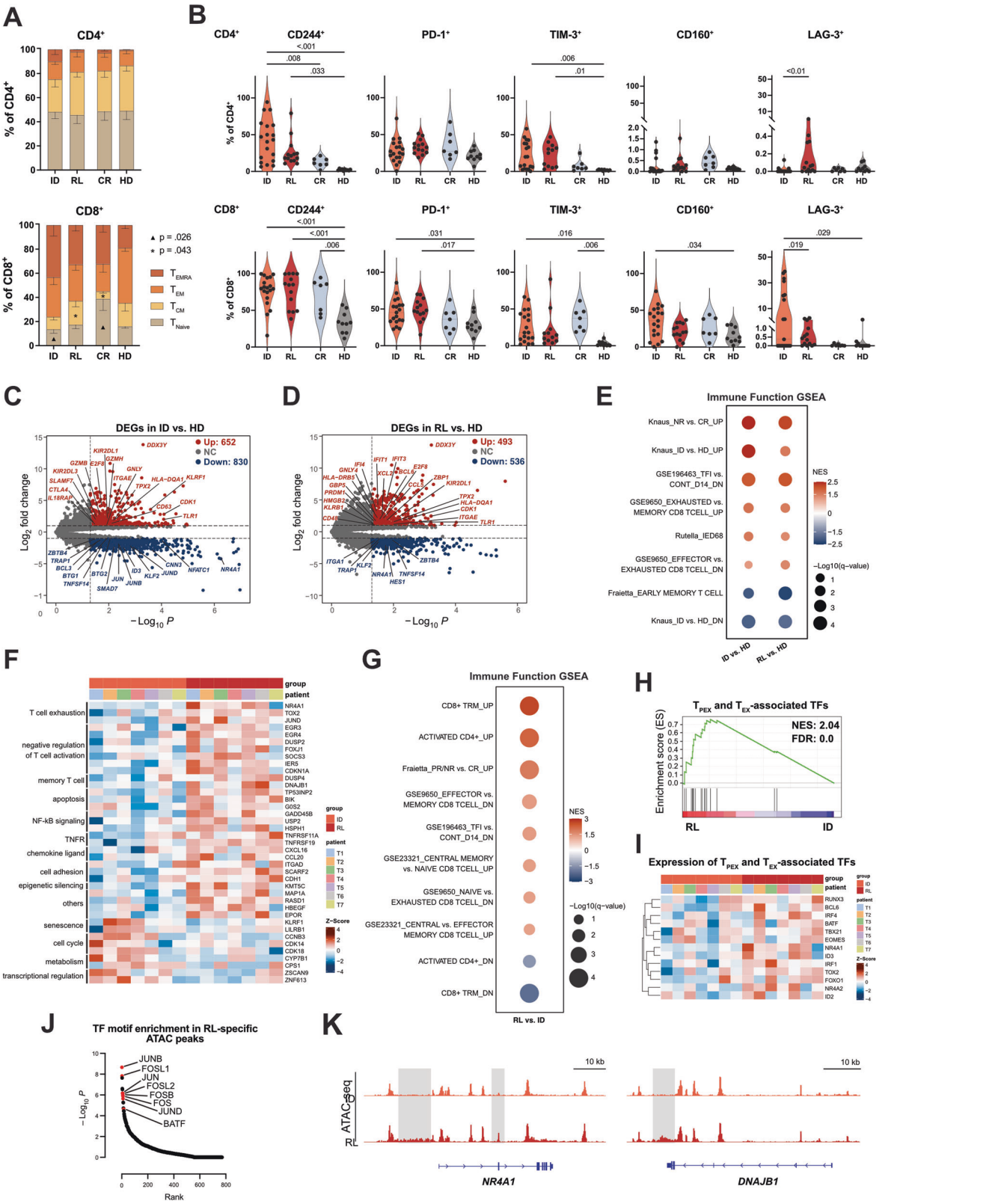

$P < 0.05$; Supplementary Table 3; Fig. 1C, D, Supplementary Fig. S2A–D), respectively. We observed upregulation of both stimulation as well as dysfunction-associated genes in ID and RL compared to HDs (ID: *CD63*, *GZMH*, *IL18RAP*, *GZMB*, *CTLA4*; RL: *BLIMP-1*, *CCL5*, *CD48*, *KLRB1*; both ID and RL: *GNLY*, *TLR1*). This finding was confirmed by gene set enrichment analysis (GSEA) using published gene sets (Supplementary Methods). Moreover, BM T cells at ID vs. HDs significantly expressed senescence-

Fig. 1 Bone marrow T cells at the time of ID and RL display a phenotypic and transcriptional profile of dysfunction. A Proportions of naive (T_{Naive}, $CD45RA^+CCR7^+$), central memory (T_{CM}, $CD45RA^-CCR7^+$), effector memory (T_{EM}, $CD45RA^-CCR7^-$), and terminal effector (T_{EMRA}, $CD45RA^+CCR7^-$) T cells within the $CD4^+$, and $CD8^+$ compartments. **B** Frequency of BM $CD4^+$ (top row) and $CD8^+$ (bottom row) T cells positive for inhibitory receptors at ID ($n = 19$), RL ($n = 14$), CR ($n = 7$), and in HDs ($n = 10$). **C** Volcano plot of DEGs at ID ($n = 7$) vs. HDs ($n = 2$). Significantly upregulated (red) and downregulated (blue) genes at ID are highlighted ($log_2FC > 1$ or < -1; $P < 0.05$). Selected genes are labeled. **D** Volcano plot of DEGs at RL ($n = 7$) vs. HDs ($n = 2$). **E** GSEA for gene sets associated with immune function using published gene sets derived from MSigDB or custom gene sets. GSEA statistics are provided in Supplementary Table 3. **F** Heatmap demonstrating selected DEGs at RL compared to ID. **G** GSEA in RL vs. ID T cells for gene sets associated with T-cell populations and immune function from MSigDB and published data sets (details on the gene sets are provided in the Supplementary Methods). GSEA statistics are included in Supplementary Table 6. **H** GSEA in RL vs. ID T cells for TFs related to T_{PEX} and T_{EX}. **I** Heatmap showing the expression of top hits, from the analysis in panel H, in ID and RL patients. **J** TF motifs enriched in RL-specific ATAC peaks. Significant motifs are labeled and highlighted in red. **K** ATAC-seq tracks of selected genes significantly upregulated in RL vs. ID T cells. BM bone marrow, CR complete remission, DEG differentially expressed gene, GSEA gene set enrichment analysis, HD healthy donor, ID initial diagnosis, RL relapse, TF transcription factor. All plots represent the mean ± SEM. One-way ANOVA was used to calculate *P* values.

associated genes like *KLRF1*, and the inhibitory KIRs (*KIR2DL3* and *KIR2DL1*). Notably, the immune effector dysfunction score (IED68) [14] demonstrated significant positive enrichment in ID vs. HD T cells in line with higher expression of senescence-associated markers at this time point (Fig. 1E, Supplementary Fig. S2E–G, Supplementary Table 4).

To elucidate the longitudinal transcriptional changes occurring in patients' T cells between ID and RL, we compared T cells from AML patients at RL ($n = 7$) to their matched ID counterparts. Differential gene expression analysis ($log_2FC > 1$ or < -1, $P < 0.05$; Supplementary Table 5) revealed high expression of senescence markers (*KLRF1*, *LILRB1*) at ID vs. RL and genes related to memory T cells (*DUSP4*, *DNAJB1*) and exhaustion (*NR4A1*, *TOX2*, *JUND*) at RL vs. ID (Fig. 1F, Supplementary Fig. S3A). GSEA indicated that pathways associated with senescence (oxidative phosphorylation and protein secretion) were enriched in ID T cells, whereas RL T cells showed enrichment for T_{CM} and tissue-resident memory T-cell (T_{RM}) signatures, as well as pathways implicated in T-cell exhaustion (Fig. 1G, Supplementary Fig. S3B; Supplementary Table 6). Accordingly, expression of core TFs associated with progenitor exhausted (T_{PEX}) and terminally exhausted T cells (T_{EX}) was significantly enhanced in RL but not ID T cells (Fig. 1H and I, Supplementary Fig. S3C, Supplementary Table 7).

We next looked at active regulatory regions in ID vs. RL T cells. ATAC-seq performed in paired ID and RL T cells identified 1294 differential ATAC peaks ($log_2FC > 1$, $P < 0.01$). The principal component analysis separated ID and RL T cells (Supplementary Fig. S3D–F). Notably, accessible regions in RL (RL-specific ATAC peaks) corresponded to changes in TF activity. TF motif analysis on these regions revealed enrichment for AP1 family TF-binding motifs (Fig. 1J, Supplementary Table 8). These findings were in line with higher expression of AP-1 and IRF family members in RL vs. ID T cells (Supplementary Fig. S3G). Furthermore, RL-specific ATAC peaks included the exhaustion-associated gene NR4A1 and the memory-associated gene DNAJB1, which were both transcriptionally upregulated in RL compared to ID T cells (Fig. 1F, K). For regions with decreased accessibility in RL T cells, we did not observe a clear pattern connected to gene expression. Together, these data demonstrate that T cells in AML bear different states of T-cell dysfunction, with senescence appearing to be more prominent at ID, whereas RL T cells exhibit a profile of exhaustion.

Next, we investigated the function of BM T cells during AML progression in vitro. At ID, T cells showed lower CD3xCD33 BiTE (AMG330)-mediated cytotoxicity and T-cell proliferation against the AML cell line (OCI-AML3) relative to RL T cells (Fig. 2A–C; Supplementary Fig. S4A–C). These findings were further validated in cocultures with primary AML cells and autologous T cells; again, ID T cells showed inferior AMG330-mediated cytotoxicity and proliferation compared to RL (Fig. 2D, E, Supplementary Fig. S4D). To study the long-term function of ID and RL T cells, we used our previously established in vitro exhaustion model system, which provides continuous exposure to the CD3xCD19 BiTE (AMG 562) in the presence of the B-cell lymphoma cell line OCI-Ly1 [11]. Indeed, we observed a higher frequency of $CD4^+$ and $CD8^+$ T cells co-expressing PD-1, TIM-3, and LAG-3 at time of ID and RL compared to CR (Fig. 2F). Similar to the short-term stimulation, ID T cells showed lower cytotoxic function and proliferation relative to RL against OCI-Ly1 cells (Fig. 2G, Supplementary Fig. S4E). However, ID and RL T cells both showed less IFN-γ and GZMB production compared to T cells from CR (Fig. 2H). By assessing the metabolic activity, we observed that T cells at ID and RL showed lower mitochondrial respiration and glycolysis relative to CR. Interestingly, metabolic impairment was more prominent in T cells at RL, as evidenced by a significantly lower spare respiratory capacity (SRC) and glycolytic reserve (Fig. 2I, J). Together, these data show that after continuous BiTE stimulation cells at ID and RL exhibited decreased effector molecule production and impaired metabolic fitness in comparison to CR. Further examination of T-cell function using CD3 and CD28 beads revealed that the addition of CD28 co-stimulation, compared to BiTE-mediated T-cell activation, improved but did not fully rescue T-cell proliferation at ID and RL relative to CR (Supplementary Fig. S5A, B).

Taken together, our study provides insights into the dysfunctional state of BM T cells and the molecular determinants of their function during AML progression. Although ELN risk group attribution was well-balanced in our analyses (Supplementary Table 9), we acknowledge that genetic heterogeneity might still impose a bias. The impaired function of T cells during active disease, either at time of ID or RL, and their functional reinvigoration at first CR support the use of BiTE molecules in patients in CR. Although limited, the lessons from clinical trials so far in R/R AML patients have indicated a better clinical response to AMG 330 and CAR T cells preferentially in patients with low disease burden [15]. Thus, promoting BiTE molecules to consolidation, for example, after first-line therapy in patients at CR with MRD positivity, with restored T-cell function and favorable E:T ratio appears to be a better-suited scenario.

It is of high importance that clinical trials evaluating these therapies incorporate thorough biomarker studies, including BM biopsies to obtain a T-cell signature associated with response to treatment. These findings then need to be integrated into clinical trials, as it is likely that the one-size-fits-all approach does not apply.

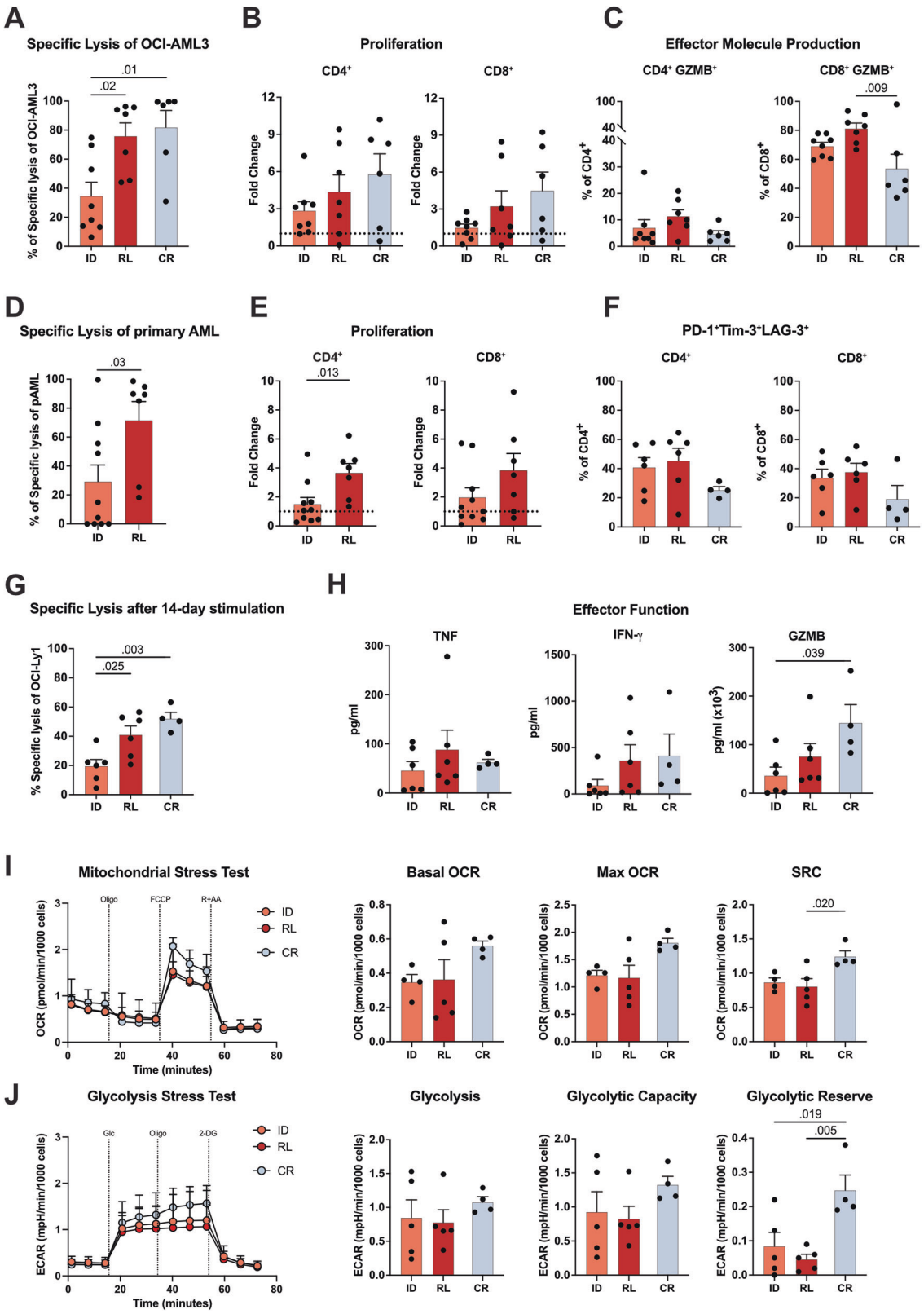
A
Specific Lysis of OCI-AML3
% of Specific lysis of OCI-AML3
.01
.02
ID
RL
CR
B
Proliferation
CD4+
CD8+
Fold Change
C
Effector Molecule Production
CD4+ GZMB+
CD8+ GZMB+
% of CD4+
% of CD8+
.009
D
Specific Lysis of primary AML
% of Specific lysis of pAML
.03
E
Proliferation
.013
F
PD-1+Tim-3+LAG-3+
G
Specific Lysis after 14-day stimulation
% Specific lysis of OCI-Ly1
.003
.025
H
Effector Function
TNF
IFN-γ
GZMB
pg/ml
pg/ml (x10^3)
.039
I
Mitochondrial Stress Test
OCR (pmol/min/1000 cells)
Oligo
FCCP
R+AA
Time (minutes)
Basal OCR
Max OCR
SRC
.020
J
Glycolysis Stress Test
ECAR (mpH/min/1000 cells)
Glc
Oligo
2-DG
Glycolysis
Glycolytic Capacity
Glycolytic Reserve
.019
.005

Fig. 2 ID T cells display lower BiTE-mediated cytotoxicity compared to RL, but both have impaired metabolic fitness after continuous stimulation. **A** AMG 330-mediated cytotoxicity of T cells sampled at ID ($n = 8$), RL ($n = 7$), and CR ($n = 6$) on day 5 against OCI-AML3 cells relative to cBiTE (concentration AMG 330 or cBiTE = 5 ng/ml, E:T = 1:3). **B** T-cell proliferation on day 5 calculated as fold change relative to the number of T cells on day 0. **C** Percentage of T cells producing GZMB measured by flow cytometry after intracellular staining on day 5. **D** AMG 330-mediated cytotoxicity of T cells sampled at ID ($n = 10$) and RL ($n = 7$) against autologous primary AML blasts in ex vivo cytotoxicity assays (concentration AMG 330 or cBiTE = 5 ng/ml) on day 6. **E** T-cell proliferation on day 6 calculated as fold change relative to the number of T cells on day 0. **F** Percentage of $CD4^+$ and $CD8^+$ T cells from patients at ID ($n = 6$), RL (n = 6), and CR (n = 4) co-expressing PD-1, Tim-3, and LAG-3 on day 14 of continuous stimulation. **G** AMG 562-mediated cytotoxicity of isolated T cells against OCI-Ly1 cells after 14 days of continuous stimulation (concentration AMG 562 or cBiTE = 5 ng/ml, E:T = 1:5, 3 days). **H** Levels of secreted TNF, IFN-γ, and GZMB measured by CBA in the supernatants of cytotoxicity assays on day 3. **I** Kinetic plot and corresponding bar graphs of normalized OCR acquired during mitochondrial stress testing of T cells from patients at ID ($n = 4$), RL ($n = 5$), and CR ($n = 4$) after 14 days of continuous stimulation with AMG 562. **J** Kinetic plot and corresponding bar graphs of normalized ECAR obtained during glycolysis stress testing of T cells from patients at ID ($n = 4$), RL ($n = 5$), and CR ($n = 4$) after 14 days of continuous stimulation with AMG 562. CR complete remission; ID initial diagnosis, RL relapse. Bar plots represent the mean ± SEM. One-way ANOVA (**A**–**C** and **F**–**J**) and Mann–Whitney tests (**D**, **E**) were used to calculate *P* values.

DATA AVAILABILITY

The RNA-seq and ATAC-seq data discussed in this publication have been deposited in the GEO database under the accession codes GSE261000 and GSE260999, respectively. The datasets generated and/or analyzed during the study are available from the corresponding author on reasonable request.

REFERENCES

1. Schmid C, Labopin M, Schaap N, Veelken H, Schleuning M, Stadler M, et al. Prophylactic donor lymphocyte infusion after allogeneic stem cell transplantation in acute leukaemia—a matched pair analysis by the Acute Leukaemia Working Party of EBMT. Br J Haematol. 2019;184:782–7.
2. Kantarjian H, Stein A, Gökbuget N, Fielding AK, Schuh AC, Ribera J-M, et al. Blinatumomab versus Chemotherapy for Advanced Acute Lymphoblastic Leukemia. N Engl J Med. 2017;376:836–47.
3. Budde LE, Assouline S, Sehn LH, Schuster SJ, Yoon SS, Yoon DH, et al. Single-agent mosunetuzumab shows durable complete responses in patients with relapsed or refractory B-cell lymphomas: phase I dose-escalation study. J Clin Oncol. 2022;40:481–91.
4. Krupka C, Kufer P, Kischel R, Zugmaier G, Bögeholz J, Köhnke T, et al. CD33 target validation and sustained depletion of AML blasts in long-term cultures by the bispecific T-cell–engaging antibody AMG 330. Blood. 2014;123:356–65.
5. Augsberger C, Hänel G, Xu W, Pulko V, Hanisch LJ, Augustin A, et al. Targeting intracellular WT1 in AML with a novel RMF-peptide-MHC-specific T-cell bispecific antibody. Blood. 2021;138:2655–69.
6. Ravandi F, Walter RB, Subklewe M, Buecklein V, Jongen-Lavrencic M, Paschka P, et al. Updated results from phase I dose-escalation study of AMG 330, a bispecific T-cell engager molecule, in patients with relapsed/refractory acute myeloid leukemia (R/R AML). J Clin Oncol. 2020;38:7508–7508.
7. Subklewe M, Stein A, Walter RB, Bhatia R, Wei AH, Ritchie D, et al. Preliminary results from a phase 1 first-in-human study of AMG 673, a novel half-life extended (HLE) anti-CD33/CD3 BiTE® (Bispecific T-Cell Engager) in patients with relapsed/refractory (R/R) acute myeloid leukemia (AML). Blood. 2019;134:833.
8. Uy GL, Aldoss I, Foster MC, Sayre PH, Wieduwilt MJ, Advani AS, et al. Flotetuzumab as salvage immunotherapy for refractory acute myeloid leukemia. Blood. 2021;137:751–62.
9. Zhao Y, Aldoss I, Qu C, Crawford JC, Gu Z, Allen EK, et al. Tumor-intrinsic and -extrinsic determinants of response to blinatumomab in adults with B-ALL. Blood. 2021;137:471–84.
10. Corrado F, Wulf J, Straub T, Nixdorf D, Marcinek A, Philipp N, et al. Single-cell transcriptomic profiling of T cells from blinatumomab-treated patients with B-cell precursor acute lymphoblastic leukemia (BCP-ALL) reveals circulating CD8 T cell subsets associated with treatment response. Blood. 2023;142:600.
11. Philipp N, Kazerani M, Nicholls A, Vick B, Wulf J, Straub T, et al. T-cell exhaustion induced by continuous bispecific molecule exposure is ameliorated by treatment-free intervals. Blood. 2022;140:1104–18.
12. Williams P, Basu S, Garcia-Manero G, Hourigan CS, Oetjen KA, Cortes JE, et al. The distribution of T-cell subsets and the expression of immune checkpoint receptors and ligands in patients with newly diagnosed and relapsed acute myeloid leukemia. Cancer. 2019;125:1470–81.
13. Belmontes B, Sawant DV, Zhong W, Tan H, Kaul A, Aeffner F, et al. Immunotherapy combinations overcome resistance to bispecific T cell engager treatment in T cell–cold solid tumors. Sci Transl Med. 2021;13:1524.
14. Rutella S, Vadakekolathu J, Mazziotta F, Reeder S, Yau T-O, Mukhopadhyay R, et al. Signatures of immune dysfunction predict outcomes and define checkpoint blockade-unresponsive microenvironments in acute myeloid leukemia. J Clin Invest. 2022;132:223.
15. Subklewe M, Bücklein V, Sallman D, Daver N. Novel immunotherapies in the treatment of AML: is there hope? Hematology. 2023;2023:691–701.

ACKNOWLEDGEMENTS

This work was supported by a Deutsche Forschungsgemeinschaft (DFG, German Research Foundation) research grant provided within the Sonderforschungsbereich SFB-TRR 388/1 2021 – 452881907 (to MS), and DFG research grant 451580403 (to MS and MK). The work was further supported by the Bavarian Elite Graduate Training Network (to MS), the Wilhelm-Sander Stiftung (to MS, project no. 2023.004.1), the Else-Kröner-Fresenius Stiftung (to MS), the Bavarian Center for Cancer Research (BZKF, to MS). We acknowledge the Flow Cytometry Core Facility at the Biomedical Center, Ludwig Maximilian University (LMU), Munich and the iFlow Core Facility of the University Hospital, LMU Munich (INST 409/225-1 FUGG) for assistance with generating the flow cytometry data. Furthermore, we thank Sabine Sandner-Thiede, Simone Pentz, Elke Habben, Ewelina Zientara, and Bianca Kirschbaum (University Hospital, LMU Munich) for their excellent technical support. We especially thank Prof. Dr. Torsten Haferlach at MLL Münchner Leukämielabor for his support with primary materials.

AUTHOR CONTRIBUTIONS

MS and MK designed the study and supervised the project; MK, NP, VLB, and MS wrote the manuscript; MK, AM, NP, BB, and JJT performed the experiments and analyzed and/or interpreted the data; MS, VLB, RK, MK, AM, NP, and BB were involved in research design and data interpretation; BT, LR, YW, MW, AJE, GM, KS, and TH were involved in the collection of samples. HDM performed ATAC-seq; MK, AT, and GS conducted ATAC-Seq bioinformatic analysis. MK performed the library preparation for bulk RNA-Seq and, in collaboration with TS, conducted the bioinformatic analysis. All authors contributed to the manuscript and approved the submitted version.

FUNDING

Open Access funding enabled and organized by Projekt DEAL.

COMPETING INTERESTS

MS has received industry research support from Amgen, BMS/Celgene, Gilead/Kite, Miltenyi Biotec, Molecular Partners, Morphosys, Novartis, Roche, Seattle Genetics, and Takeda, and has served as a consultant/scientific advisory board member at Autolus, AvenCell, CanCell Therapeutics, CDR-Life, Genmab US, Ichnos Sciences, Incyte Biosciences, Interius BioTherapeutics, Janssen, Millennium Pharmaceuticals, Miltenyi Biomedicine, Molecular Partners, Nektar Therapeutics, Novartis, Pfizer, Ridgeline Discovery, Sanofi, Scare, and Takeda. She serves on the speakers' bureau at Amgen, AstraZeneca, BMS/Celgene, Gilead/Kite, GSK, Janssen, Novartis, Octapharma, Pfizer, Roche, Springer Healthcare, and Takeda. Educational grants were received to develop the app "MyTcell" from BMS, Gilead, Janssen, Novartis, Roche, and Takeda. VLB has received research funding from BMS, Gilead/Kite, Miltenyi Biotec, Novartis, and Roche, and has served as a consultant/advisor to Amgen, Gilead, Novartis, Pfizer, and Priothera. He serves on the speakers' bureau at Novartis and Pfizer. RK is employed at Amgen Research Munich, Germany. ST has served as a consultant/advisor to Amgen, BMS, GSK, Janssen, Pfizer, Sanofi, and Takeda. TH has received industry research support from Roche and served as a scientific advisory board member to Servier. MK, AM (now employed by MLL Munich Leukemia Laboratory), NP, BB (now employed by Adivo), JJT (now employed by AstraZeneca), HDM (now employed by MundiCare), AT, BT, LR, YW, MW, A-JE, GM, KS, TS, and GS declare no relevant conflicts of interest.

Correspondence: Marion Subklewe, Department of Medicine III, University Hospital, LMU Munich, Munich, Germany; e-mail: marion.subklewe@med.uni-muenchen.de.

ADDITIONAL INFORMATION

Supplementary information The online version contains supplementary material available at https://doi.org/10.1038/s41375-024-02387-4.

Correspondence and requests for materials should be addressed to Marion Subklewe.

Reprints and permission information is available at http://www.nature.com/reprints

Publisher's note Springer Nature remains neutral with regard to jurisdictional claims in published maps and institutional affiliations.